1. Omar H. Salim [1], 2. Yasir M.Y. Ameen [2]

University of Mosul (1,2)
ORCID: 1. 0000-0002-3863-8259; 2. 0000-0002-2878-8165

doi:10.15199/48.2023.05.06

DC-Coupled Extreme Fast Charging for Electric Vehicles Using DAB Converter

Abstract. *Currently, long charging times are a major problem hindering the spread of electric vehicle (EV) technology. This paper develops a DC-coupled bidirectional extreme fast charger (XFC) for EVs with a power range of 1.4 MW, and an output voltage range of 1500 V, the highest charging voltage within the CHAdeMO standard. The dual active bridge (DAB) converter serves as the foundation of the developed XFC's multi-level structure. It has proven feasible to integrate Energy Storage Systems (ESS) with DC renewable energy sources for each level of the converter, eliminating the AC-AC stage from the conventional XFC design and resulting in a smaller load size at a lower cost. The presented XFC is simulated using MATLAB/Simulink. The findings shown that using the constant-current constant-voltage (CCCV) charging method based on two nested PI controllers, the heavy vehicle battery pack with a capacity of 540 kWh could be charged from 20% to 90% state of charge (SOC) in as little as 18 minutes and 40 seconds. A prototype 1 kW bidirectional DAB converter laboratory model with SiC MOSFET switches was created and demonstrated. The outcomes of the practical part were in good agreement with those of the simulation and mathematical analysis*

Streszczenie. *Obecnie dużym problemem utrudniającym rozprzestrzenianie się technologii pojazdów elektrycznych (EV) są długie czasy ładowania. W niniejszym artykule opracowano dwukierunkową ekstremalnie szybką ładowarkę (XFC) sprzężoną z prądem stałym do pojazdów elektrycznych o mocy 1,4 MW i zakresie napięcia wyjściowego 1500 V, które jest najwyższym napięciem ładowania w standardzie CHAdeMO. Konwerter z podwójnym aktywnym mostkiem (DAB) służy jako podstawa opracowanej wielopoziomowej struktury XFC. Integracja systemów magazynowania energii (ESS) z odnawialnymi źródłami energii DC na każdym poziomie przekształtnika okazała się wykonalna, eliminując stopień AC-AC z konwencjonalnej konstrukcji XFC i powodując mniejszy rozmiar obciążenia przy niższych kosztach. Prezentowany XFC jest symulowany za pomocą MATLAB/Simulink. Z badań wynika, że przy użyciu metody ładowania stałym prądem stałym napięciem (CCCV) opartej na dwóch zagnieżdżonych regulatorach PI, pakiet akumulatorów pojazdów ciężkich o pojemności 540 kWh może być ładowany od 20% do 90% stanu naładowania (SOC). w zaledwie 18 minut i 40 sekund. Stworzono i zademonstrowano prototypowy model laboratoryjny dwukierunkowego konwertera DAB o mocy 1 kW z przełącznikami SiC MOSFET. Wyniki części praktycznej były zgodne z wynikami symulacji i analizy matematycznej* (***Ekstremalnie szybkie ładowanie ze sprzężeniem DC dla pojazdów elektrycznych za pomocą konwertera DAB***)

Keywords: DAB Converter, Extreme Fast Charging, CHAdeMO, CCCV, V2G, ZVS.
Słowa kluczowe: Konwerter DAB, ekstremalnie szybkie ładowanie, CHAdeMO, CCCV, V2G, ZVS.

Introduction

As the negative effects of the fossil fuel-based transportation industry have come to light, people, businesses, and governmental organizations have made a determined effort to find solutions to provide a less carbon-intensive means of transportation. Importantly, the sale of automobiles with internal combustion engines will come to an end in the European Union in 2035, hastening the transition to electric vehicles (EVs). Many innovative steps have been employed in recent decades to lower the price of EVs while increasing their range. Nevertheless, new advancements in lithium-ion battery technology aim to build vehicles with even higher ranges while also reducing the price and weight of the batteries. Meanwhile, the newer batteries' acceptance of charge amounts is improving steadily, enabling significantly faster charge rates. However, EVs can be charged using AC charging or DC charging systems [1]. The DC charging system, unlike the AC charging technology, charges the battery directly from the DC charging station, bypassing any onboard AC-DC converter (if any). The DC charging system, also known as the off-board charger, charges EVs far more quickly than AC chargers since it can deliver high power without requiring any modifications or adaptations to the EVs. Therefore, the DC charging system has attracted a lot of attention, and a network of DC fast charging stations are often found on major highways for long-distance driving. In this context, active research efforts have been made to reduce the EV battery charging time while increasing a charging station's throughput reduces the need for as many chargers at each charging station [2]. However, the increasing number of EVs and the different charging requirements of the manufacturers posed another challenge for researchers and developers of chargers. As a result, several governing bodies have developed standardized charging protocols to ensure compatibility and safety with charging systems. The one of these organizations. It created a standard charging protocol and classified it into three AC charging modes and one DC charging mode (mode 4) which provides a maximum charging power of 400 kW (1000 V, 400 A). Whereas society of automotive engineers (SAE) in North America classified the chargers into four levels, two levels for AC charging, and two for DC charging with a power capacity of 40 kW (500 V, 80 A) in DC level 1 and 100 kW (500 V, 200 A) in DC level 2. Guobiao (GB) standards are the Chinese national standards, which created GB/T 20234 family for EV charging infrastructures. The DC charging standard (GB/T 20234.3) supports up to 250 kW (1000 V, 250 A). In the meantime, the CHAdeMO standard was developed by Japanese firms, including Nissan and Mitsubishi. CHAdeMO serves the greatest number of fast-charging plug-ins globally. CHAdeMO/CHAoji serves a maximum power of 900 kW (1500 V, 600 A) of high-voltage DC fast charging. Table 1 summarizes the standards for DC fast charging.

Table 1. Standards for DC fast charging [3]–[6]

Standard	**Category**	**Max charger Voltage (V)**	**Max charger Current (A)**	**Max charger Power (kW)**
IEC-62196	MODE 4	1000	400	400
SAE J1772	DC LEVEL1	200-500	80	40
	DC LEVEL2	200-500	200	100
GB/T-20234.3-2015	DC	750-1000	250	250
CHAdeMO	1.0	500	125	62.5
	1.2	500	400	200
	2.0	1000	400	400
	3.0	833	600	500
	CHAoji	1500	600	900

Unlike others, Tesla refers to its own fast charging stations as Supercharger stations. In fact, it is not itself an international standard. Nevertheless, Tesla reports peak charging power for its V3 superchargers that can reach 250 kW (315 V, 800 A).

From the viewpoint of this work, Table 2 summarizes the basic characteristics of earlier studies as well as their key limitations. The majority of early works in the literature had either a low power rating or unidirectional power flow with no protection against overcharging. In addition, some of these works were complicated in terms of transformer design or control.

Consequently, the purpose of this paper is to show the design, simulation, and implementation of a bidirectional XFC 1.4 MW at 1500 V, which is the maximum allowed voltage so far according to the CHAdeMO standard. The developed XFC is based on an isolated DAB converter using a phase shift modulation technique. The adopted charger topology does not require the use of a line-frequency transformer stage, thereby reducing the charger's size, weight, and cost. However, the methodology and procedures of the present paper with the sub-goals to achieve the main design goal of the proposed XFC can be summarized as follows:

• A mathematical analysis of the DAB-based XFC is performed to get an idea of the voltages, currents and power control parameters of the charger;

• A simulation using the MATLAB Simulink platform is performed to evaluate the performance of the proposed XFC.

• Experimental laboratory tests are performed to validate the mathematical analysis and simulation results.

Table 2. Comparison of basic features of previous research

Ref.	DC-DC topology	Switches Number per module	diode	Power (kW)	Experimental	Galvanic Isolation	bidirectional	Main limitation compared to the present work
[7]	BUCK	1	1	50	n	n	y	Low power, no insolation
[8]	NPC	4	6	50	y	y	n	Low power, unidirectional
[9]	IUDB	4	4	50	n	y	n	
[10]	PSFB	4	4	50	n	y	n	
[11]	modified topology	8	12	240	n	y	n	unidirectional
[12]	DAB and PPCU	16	10	6*350	y	y	n	Unidirectional, more complicated and include more circuits, 4.4C charging
[13]	SEPIC	3	3	600	y	y	n	unidirectional 10C charging, cc-mode only
[14]	QAB	16	0	1000	y	y	y	HFT required an additional balancing winding
Present work	DAB	8	0	1417	y	y	y	--

The architecture of XFC

The charging rate of EVs refers to the time required to charge the EVs battery. Slow charging is defined as taking more than an hour to charge the battery or the charging current is less than 1C per hour. Fast charging is defined as taking less than an hour of charging or the charging current is more than 1C per hour, while XFC takes less than twenty minutes or the charging current is more than 3C per hour [15]. Where C is defined as the nominal capacity of the battery and is measured in ampere-hours.

Conventional DC fast chargers for EVs require three stages to connect to medium voltage alternate current (MVAC). as shown in Fig. 1. The first stage is the line frequency transformer, which converts an AC voltage from one level to another AC voltage level via a conventional low-frequency transformer (LFT). It is typically used to step down (MVAC) to a low AC voltage and provide galvanic isolation. The second stage is the AC-DC rectifier via power electronics circuits. This stage has particular drawbacks in high-power charging processes with the MW range as producing unwanted harmonic effects, and this stage also requires protection devices and more complex control strategies, a power factor correction is usually included in this stage [16]. The third stage is a DC-DC converter via power electronics to convert the intermediate DC voltage to the DC voltage level required to charge the EV pack battery. Galvanic insulation is not required at this stage as it was provided in the first phase transformer according to this architecture. However, the first and second stages of the XFC structure can be eliminated if the main DC input of the last stage is taken directly from a DC source such as a solar cell power plant. Regardless, the design considerations of the first and second stages are not the subject of this study.

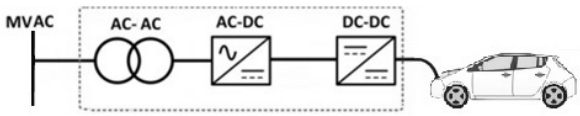

Fig. 1 The architecture of conventional XFC

In any case, most of these chargers are designed to flow power unidirectionally from the grid to vehicle G2V. It has a simpler structure than bidirectional chargers that offer greater advantages by inverting power flow from vehicle to everything (V2X), from the vehicle to grid V2G or to a home load V2H or even vehicle to vehicle V2V.

DC-DC converters

There is a wide range of isolated DC-DC converters available mainly for low power applications such as flyback, forward and ZETA that feature simple circuit design and few switches. However, these converters suffer from many limitations that make them unsuitable for XFC applications.

Meanwhile, a single-phase dual active bridge (DAB) has many characteristics that make it a suitable choice for XFC technology. It has high power density, relatively simple control, fewer passive components, galvanic isolation of the input/output sides, the possibility of connection to medium-voltage networks and the ability to work in both directions to transmit the power [17]. In addition, it can provide a wide range of output voltage whether in step-up mode or step-down mode. Moreover, DAB has good switching characteristics by distributing even currents to the switches and achieving smooth switching of power semiconductor devices. Another preferred feature of DAB is its ability to operate at high switching frequencies with high efficiency, thereby reducing the size of the high frequency transformer (HFT) as well as the overall size of the converter.

The structure of the DAB converter can be divided into three stages. The DC-AC stage, the AC-AC power conversion stage with HFT, and the AC-DC stage. DAB converter contains two full H-bridge circuits connected to the leakage inductance (L) and a HFT as indicated in Fig. 2.

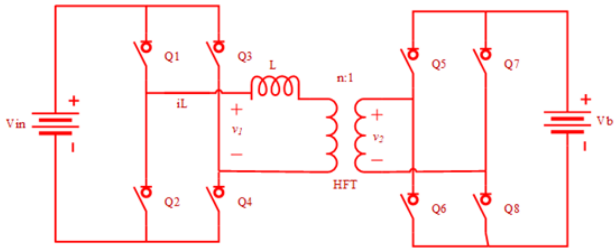

Fig. 2 The DAB topology

As already mentioned, the switchovers in DAB can be seamless. For example, when MOSFETs are used as the conversion switches in the DAB circuit, a zero voltage switching (ZVS) soft transition occurs when the drain-source voltage is almost zero before the switch turns on. However, to achieve ZVS in the DAB converter, the values of inductance and dead time of each H-bridge switch must be carefully chosen. It is important to remember that while increasing inductance helps achieve ZVS, it also increases reactive power and decreases efficiency. Similarly, a longer dead time ensures completion of the ZVS but increases the loss due to the increased lead time of the diode to the body [18].

On the other hand, various modulation approaches are used to derive DAB. The three main modulation approaches are phase-shift, trapezoidal, and triangular modulation. Simple-phase-shift modulation has a lower RMS current in leakage inductance and achieves soft-switching and high power transfer. In a phase-shift, also commonly called as the rectangular modulation approach, the direction and magnitude of energy flow are determined by a phase-shift between the input bridge and the output bridge. This difference is defined as (Ø) causing a potential difference over the leakage inductance [19]. As a result, the current is induced.

Mathematical Analysis

This section presents the mathematical analysis of phase shift modulation-based DAB when operated as a power converter of XFC. The analysis is based on the variation of converter circuit topologies for each event. Different voltages and currents are applied at various periods of a switching cycle of phase shift modulation technique-based DAB. Figs. 3, 4, 5 and 6, display the status of the switches, marking the active and inactive elements with red and black; respectively. The current flow equations for each circuit topology can be deduced as shown below each figure.

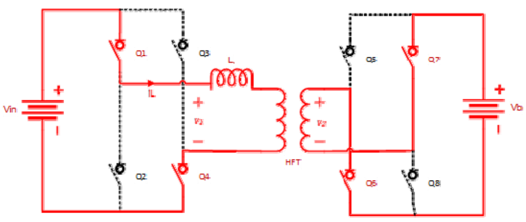

Fig. 3 DAB switches status at time interval T1

(1) $$i_L(t) = i_L(0) + \frac{1}{L}(V_{in} + nV_b)\Delta t$$

Where i_L is Leakage inductor current, V_{in} is DC input voltage, V_b is DC output voltage, and n is the HFT ratio.

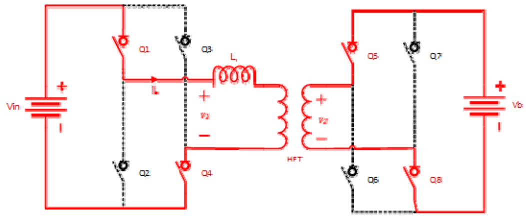

Fig. 4 DAB switches status at time interval T2

(2) $$i_L(t) = i_L(t_1) + \frac{1}{L}(V_{in} - nV_b)\Delta t$$

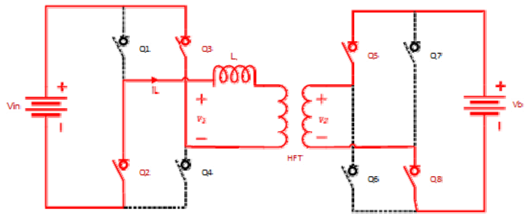

Fig. 5 DAB switches status at time interval T3

(3) $$i_L(t) = i_L(t_2) + \frac{1}{L}(-V_{in} - nV_b)\Delta t$$

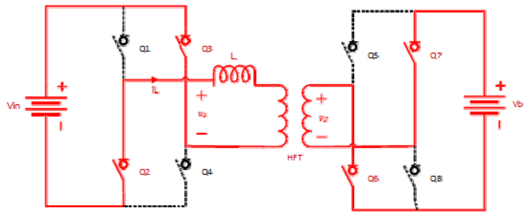

Fig. 6 DAB switches status at time interval T4

(4) $$i_L(t) = i_L(t_3) + \frac{1}{L}(-V_{in} + nV_b)\Delta t$$

However, to simplify the circuit analysis and to obtain both the output voltage and power equations, the AC voltages on the input and output H-bridges of Fig. 2 can replace their H-bridge circuits with the relevant voltage sources v_1 and v_2 as shown in Fig. 7 [20].

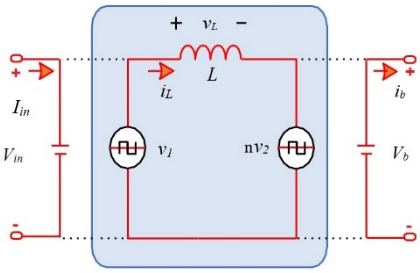

Fig. 7 The DAB equivalent circuit

Based on the last circuit simplification and the switching function analysis, the following equations are derived to control the output voltage V_o and power P [21].

(5) $$V_o = \frac{nV_{in}R_b}{2\pi f_s L}\phi(1 - \frac{\phi}{\pi})$$

(6) $$P = \frac{nV_{in}V_b}{2\pi f_s L}\phi(1 - \frac{\phi}{\pi})$$

Where R_b is battery internal resistance, and f_s is switching frequency.

The required angle for transmitting a given amount of power is thus as follows:

(7)
$$\phi = \frac{\pi \mp \sqrt{\pi^2 - \frac{8\pi^2 f_s L P}{n V_b V_{in}}}}{2}$$

The possible values of Ø = [0, π/2]. Because imaginary values for Ø are not valid, the term under the square root must not be less than zero:

(8)
$$L \le \frac{n V_b V_{in}}{8 f_s P}$$

The maximum power would be transferred at an angle of Ø = π/2 with this maximum value for the leakage inductance.

(9)
$$P_{\max} \le \frac{n V_b V_{in}}{8 f_s L}$$

Design, Simulation, and implementation of XFC

a- DAB-based XFC Designed Parameters

The proposed use of a DAB converter within the charging application eliminates the need for the AC-AC converter used in traditional fast or XFC chargers. The DAB converter incorporates the required features by adding an AC-AC transformer that provides galvanic isolation and steps down the medium voltage to the required voltage. The maximum allowed output voltage for DC EV fast chargers is 1500V based on standard CHAdeMO/CHAoji. Other parameters of the designed XFC and the used battery model are listed in Table 3.

Table 3. XFC and Battery Model Parameters

Charger Parameters	
DC Input voltage	11 kV
Max charger power	1.4 MW
Output charger voltage	900-1500 V
Max output charger current	954 A
Battery Model Parameters	
Battery capacity	540 kWh
Nominal voltage	1288 V
Fully charged voltage	1500 V
Rated capacity	419 Ah

Five modules of the DAB converter were connected input-series output-parallel (ISOP) for each phase as shown in Fig. 8, so the total connected modules of the charger system are 15 modules. This is to overcome the voltage limiters of the power electronics switches to connect the converter with the 11 kV DC supply. A SiC MOSFET type (G2R120MT33J) with a 3300V blocking voltage, 69 A at 25°C was used in this charger.

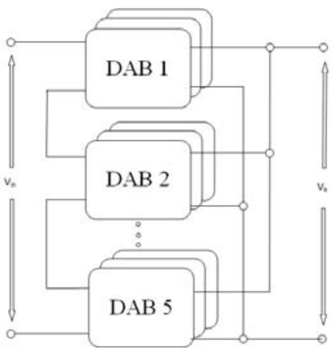

Fig. 8 ISOP DAB modular configuration

The DAB module specifications are listed in Table 4 below. The developed model of an individual DAB module in MATLAB/Simulink is shown in fig. 9.

Table 4. DAB module parameters

Item	Symbol	Value	Unit
DAB Input Voltage	V_1	2200	V
DAB Output Voltage	V_2	1500	V
Max DAB Module Power	P	94.5	kW
Switching Frequency	fs	50	kHz
Leakage Inductor	L	97.7	μH
HFT Ratio	$n:1$	7:5	--
Dab Input Capacitor	C_1	28	μF
Dab Output Capacitor	C_2	42	μF

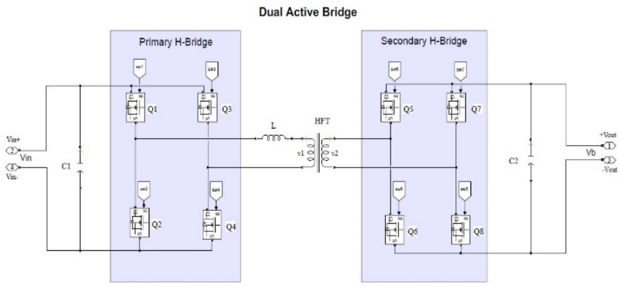

Fig. 9 Single DAB module in Simulink

Additionally, the CCCV charging method was achieved by employing two PI control circuits, which prevented the battery from increasing its current during the initial charging stage and from exceeding the maximum voltage that was recommended for it during the second stage of charging without significantly slowing down the charging process, especially in the nominal region of the battery.

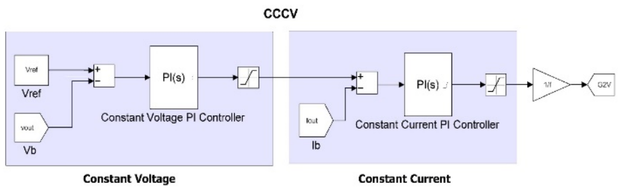

Fig. 10 Block of the cascade PI control in Simulink

For driving DAB-based XFC using a phase-shift modulation technique, Figs. 11 and 12 show a case of the necessary gate signals of the MOSFETs in the G2V and V2G operating modes; respectively. The dead time between gate signals is set to 200 ns.

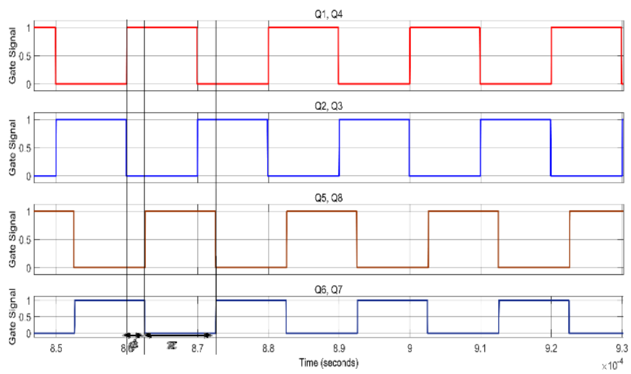

Fig. 11 SiC MOSFET pulsing signals in G2V

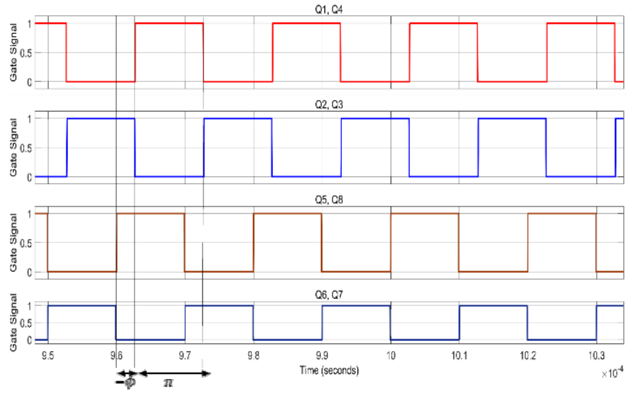

Fig. 12 SiC MOSFET pulsing signals in V2G

b- Simulation Result of DAB-based XFC

The charging speed is normally measured within the nominal area range of the battery characteristics, which is from 20% to 90% of the SOC charging state. The charging profile simulation of the XFC shown in Fig. 13 was performed within this period. The time required to charge a 540 kWh battery from 20% to 90% is only 18 minutes and 40 seconds. It can also be seen from this figure that the electric power stored in the battery is increased from 108 to 486 kWh and thus the value of the SOC state of charge on which it depends is increased.

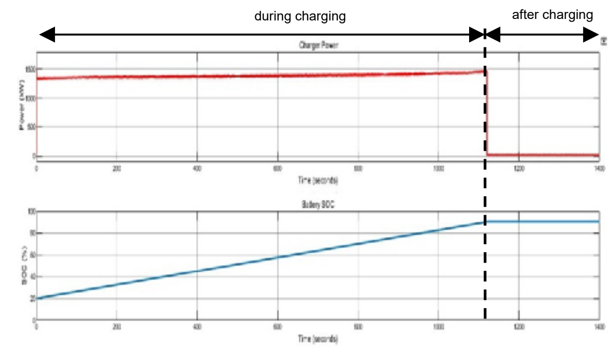

Fig. 13 Charging Profile

Fig. 14 shows a demonstration case of the G2V mode of operation for HFT primary and secondary voltages with stray coil voltage and current waveforms. the waveforms on both sides of the HFT v_1 of the primary side with a voltage of ±2200V, which is one-fifth of the total input DC voltage of 11 kV, and v_2 of the secondary side at a voltage of ±1500V and with a phase shift (Ø) between the primary and secondary sides. The voltage, v_L, and current, i_L, waveforms of the leakage inductance are also shown in Fig. 14. It can be noted that the value of vL is 4469 V during the display period T1 when the AC voltage on the primary side of the transformer v_1 is positive and the secondary side voltage v_2 is negative. This leads to a significant increase in the inductance current to reach 58 A. For the second period T2, when the voltage on both sides of the transformer is positive, the inductance voltage drops to reach 100 V, while the inductance current increases slightly to 64 A. In the third period T3, when v_1 is negative and v_2 is positive, the inductance voltage drops dramatically to -4469 V accompanied by a sharp drop in the inductance current to reach -58 A. In the latter time period T4, when the voltage is negative on both ends of the transformer, the voltage across the inductance is -100 V and the current is -64 A. Similarly, Fig. 15 shows a demonstration case of the HFT primary and secondary voltages and the stray coil voltage and current waveforms, but for the V2G mode of operation. The main difference is the negative sign of φ, which consequently lags or leads the previous waveforms compared to the waveforms of the G2V case. The output voltage and current waveforms for any DAB of the total of fifteen converters are shown in Fig.16. From this figure it can be seen that the output current for each DAB is about 63A. So, the total charging current of XFC is obtained by collecting the outputs of the fifteen DABs connected in parallel, which is 945 A, the maximum XFC current. The capacity of the XFC in this situation is 1.417 MW, which is the maximum capability of the presented XFC. According to an EV battery with a rated capacity of 419 Ah, the charging c-rate will be 2.25C.

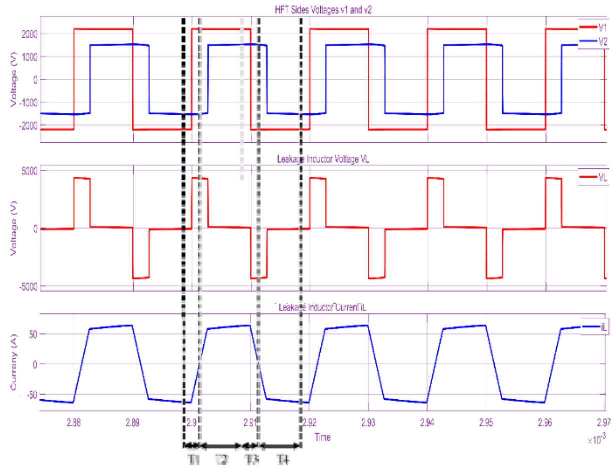

Fig. 14 HFT Primary and Secondary voltages with Leakage Inductor voltage and current waveforms in G2V

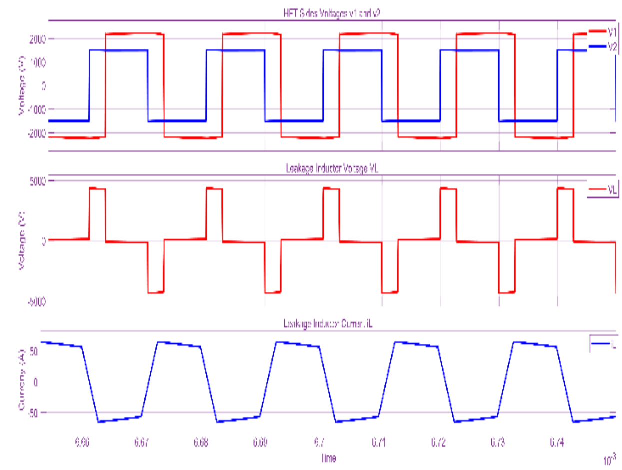

Fig. 15 HFT Primary and Secondary voltages

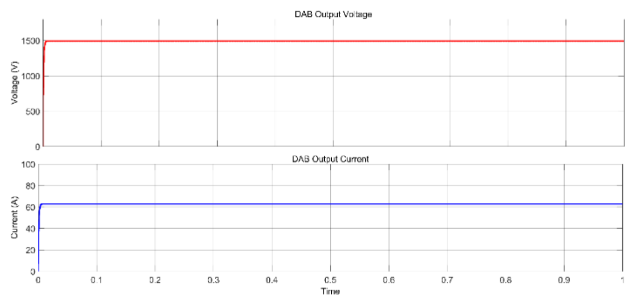

Fig. 16 DAB module output voltage and current

The gate signal, drain current ID, and drain-source voltage VDS, over the Q1 MOSFET in the primary bridge and the Q5 MOSFET in the secondary bridge are shown in Fig. 17 and Fig. 18 for a case in G2V mode and a case in V2G mode, respectively. The ZVS of both the primary and secondary H-bridge switches are evident as indicated in the relevant figures.

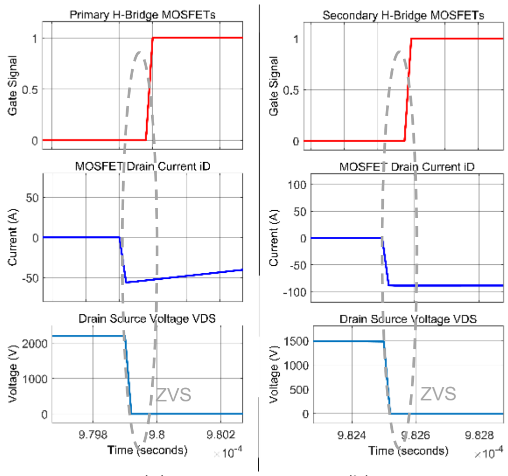

(a) (b)

Fig. 17 ZVS at switches turn on in G2V, (a) primary H-bridge MOSFETs and (b) secondary H-bridge MOSFETs

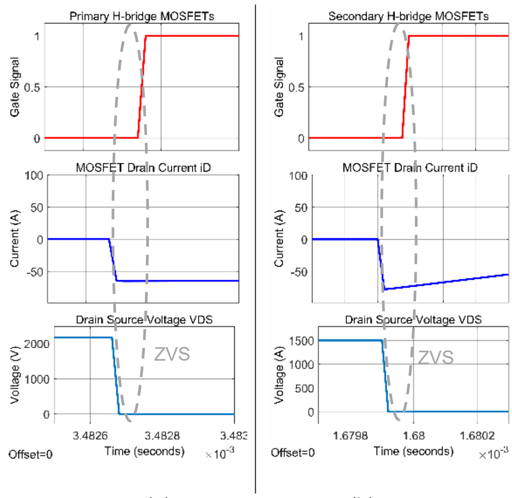

(a) (b)

Fig. 18 ZVS at switches turn on in V2G, (a) primary H-bridge MOSFETs and (b) secondary H-bridge MOSFETs

c-Implementation and validation of DAB-based XFC results.

In this section, a scaled-down prototype model of the proposed 1.4 MW 1500 V bi-directional DAB-based XFC is developed. The prototype model is scaled down to 1 kW and operates at a switching frequency of 20 kHz. The prototype model is implemented using SiC MOSFET (C2M0080120D) switches 1200V/36A at 25°C as shown in Fig. 19.

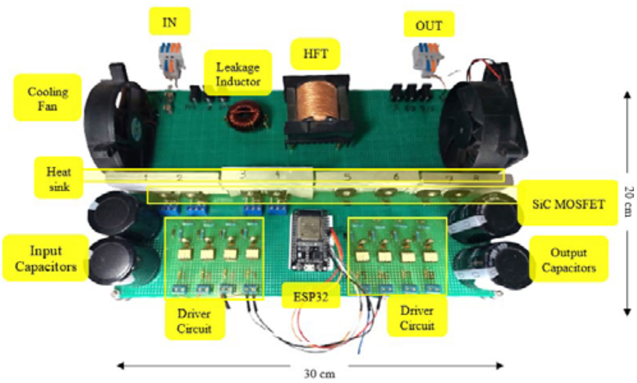

Fig. 19 DAB prototype picture

Fig. 20 shows the ESP32 controller signals used to drive the primary bridge switches at a frequency of 20 kHz based on phase shift modulation.

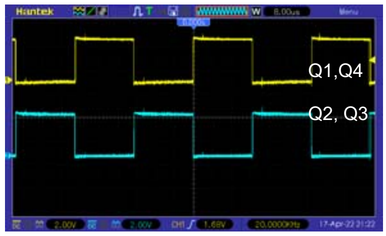

Fig. 20 Gate signals for primary bridge switches

A phase shift of 30º, 60º, 90º, and 150º is shown in Fig. 21 for the gate signals of switch Q1 in the primary bridge and its counterpart switch Q5 in the secondary bridge.

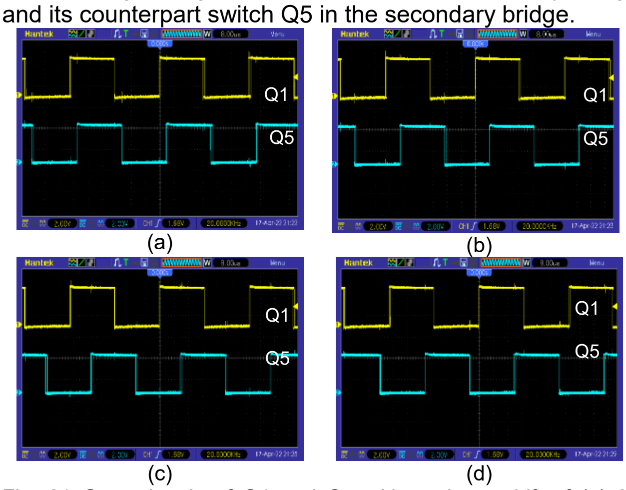

Fig. 21 Gate signals of Q1 and Q5 with a phase shift of (a) 30 degrees, (b) 60 degrees, (c) 90 degrees, and (d) 150 degrees

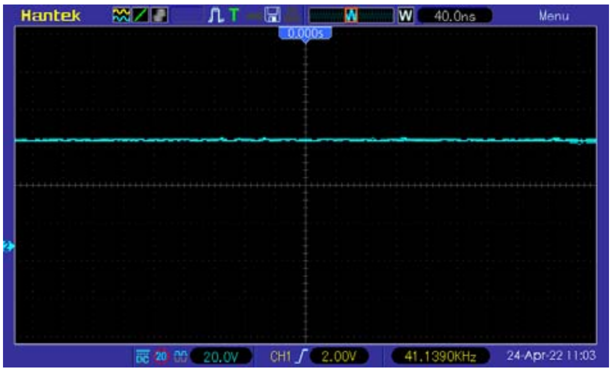

Fig. 22 DAB output voltage Vb

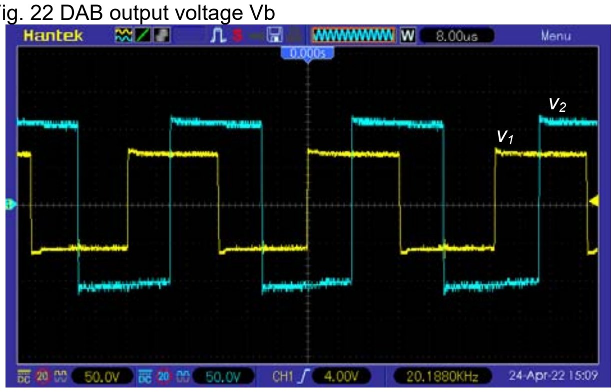

Fig. 23 The two voltages HFT sides, v1 and v2 in G2V

For the charging mode i.e., G2V, the changer output voltage, Vb, is depicted in Fig.22. Fig. 23 shows the waveforms on either side of the HFT, v1 of the primary side and v2 of the secondary side for a phase shift equal to (π/2). The voltage vL and current iL waveforms of the leakage inductor are shown in Fig. 24, where, as previously analyzed, they are synthesized by four operating segments.

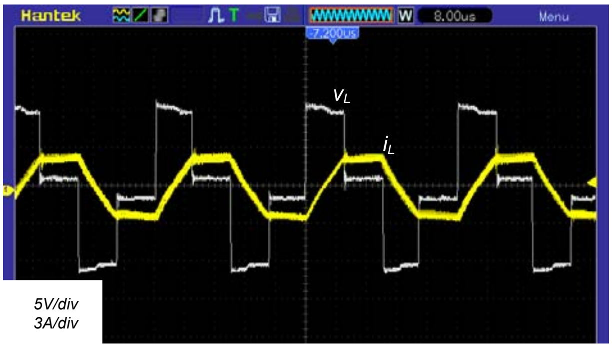

Fig. 24 The voltage vL and current iL waves of the leakage inductor in G2V

For the discharge mode i.e., V2G Fig. 25 displays the waveforms for both v1 and v2, as well as the waveform of the inductor current, i_L.

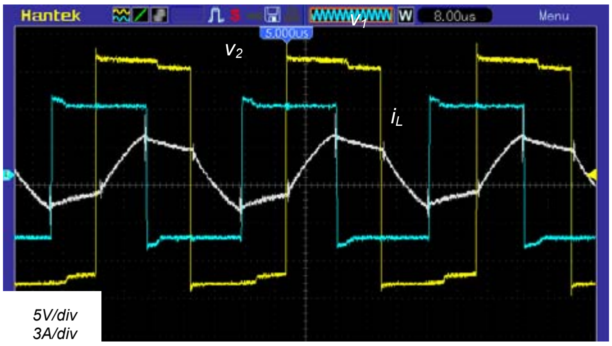

Fig. 25 The two voltages HFT sides, v1 and v2, with a leakage inductor current iL in V2G

With the input voltage Vin equal to 40 V and the switching frequency fs equal to 20 kHz, Table 5 shows the measured inductor current iL and the converter output voltage Vb for several values of phase shift angles. From this table, it can be seen that the output voltage increases as the phase shift angle increases up to 90°, where the output voltage reaches its maximum value, and then the voltages start to fall when the phase shift increases more than 90°.

Table 5. Measurement of inductor current i_L and variable output voltage V_b at several phase shift angles

Phase shift Ø (deg)	**Inductor current i_L (A)**	**Output Voltage V_b (V)**
10	2.11	32.2
30	3.69	41.3
60	4.3	50.9
90	5.2	57
120	4.21	50.8
150	3.29	40.4
170	2.46	31.7

Conclusions

The design of the XFC has shown that the proposed structure based on the DAB converter makes it possible to dispense with the line-frequency AC-AC stage, which must be present in the structure of conventional XFC, since DAB ensures the galvanic isolation between the grid side and the battery side with its ability to adapt the input voltage to the required battery charging voltage. The shortening of the AC-AC stage reduces the size and weight of the charger and also reduces its cost.

In addition, the multi-level proposed structure works by dividing the voltage between the DAB switches of each level, and thus this converter can be linked to the MVDC. DAB-based XFC has the ability to transfer power in both directions, i.e., G2V and V2G or even to another vehicle V2V.

The simulation results of the DAB-based XFC for EVs showed that the required time for charging a 540 kWh heavy-duty vehicle battery pack was reduced to only 18 minutes and 40 seconds.

The adoption of the proposed DAB-based XFC at an output voltage of 1500 V according to the CHAdeMO/CHAoji standard made it possible to reduce the maximum charging rate to 2.25 C, which is a safe charging rate to maintain longer battery life. It was found that DAB with the method of phase shift modulation achieves eight soft switching regions when starting the switches. Additionally, the CCCV charging method was achieved by employing two PI control circuits, which prevented the battery from increasing its current during the initial charging stage and from exceeding the maximum voltage that was recommended for it during the second stage of charging without significantly slowing down the charging process, especially in the nominal region of the battery.

Acknowledgments: The authors thank the University of Mosul/College of Engineering for their assistance in improving the quality of this work.

***Authors**: Omar H. Salim - E-mail: omar.20enp46@student.uomosul.edu.iq, received the B.Sc. degree from the Electrical Department, Mosul University, Iraq, where he is currently pursuing his M.Sc. degree in power electronics. He is a member in Iraqi Engineers Union (IEU) and Project Management Institute (PMI). His current research interests include the design and analysis of extreme fast charging for EV.*

Dr. Yasir M. Y. Ameen Email: yasir_752000@uomosul.edu.iq, received bachelor, master, and Ph.D. degree in Power and Electrical Machines Engineering from University of Mosul in 1997, 2000, and 2008 respectively. He is a member in Iraqi Engineers Union (IEU). He is a Lecturer in Department of Electrical Engineering. His research interests include power electronics, electrical machines and their drives. His affiliation is Department of Electrical Engineering, College of Engineering, University of Mosul, Mosul, 41001, Iraq.

REFERENCES

[1] A. Srilatha, A. Pandian, and P. S. Varma, “Review of Different Methods and Topologies for Fast Charging of Electric Vehicles,” Int. J. Res. Innov. Appl. Sci., vol. V, no. Xi, pp. 64–76, 2020, [Online]. Available: https://www.rsisinternational.org/journals/ijrias/DigitalLibrary/Vol.5&Issue11/64-76.pdf.

[2] J. Yuan, L. Dorn-Gomba, A. D. Callegaro, J. Reimers, and A. Emadi, “A review of bidirectional on-board chargers for electric vehicles,” IEEE Access, vol. 9, pp. 51501–51518, 2021, doi: 10.1109/ACCESS.2021.3069448.

[3] IEC, “IEC 61851: Electric vehicle conductive charging system,” Geneva, Switz., pp. 1–135, 2020, [Online]. Available: https://webstore.iec.ch/publication/31531#additionalinfo.

[4] H. S. Das, M. M. Rahman, S. Li, and C. W. Tan, “Electric vehicles standards, charging infrastructure, and impact on grid integration: A technological review,” Renew. Sustain. Energy Rev., vol. 120, no. February, p. 109618, Mar. 2020, doi: 10.1016/j.rser.2019.109618.

[5] “SAE Electric Vehicle and Plug in Hybrid Electric Vehicle Conductive Coupler,” SAE Int., vol. J1772_2017, pp. 1–1, doi: https://doi.org/10.4271/J1772_201710.

[6] “Connection set for conductive charging of electric vehicles --

Part 1: General requirements," CQC, 2022. http://www.cqc.com.cn/dynamic/contentcore/resource/download?ID=32242.
[7] J. Y. Yong, V. K. Ramachandaramurthy, K. M. Tan, and N. Mithulananthan, "Bi-directional electric vehicle fast charging station with novel reactive power compensation for voltage regulation," Int. J. Electr. Power Energy Syst., vol. 64, pp. 300–310, 2015, doi: 10.1016/j.ijepes.2014.07.025.
[8] S. Srdic, C. Zhang, X. Liang, W. Yu, and S. Lukic, "A SiC-based power converter module for medium-voltage fast charger for plug-in electric vehicles," Conf. Proc. - IEEE Appl. Power Electron. Conf. Expo. - APEC, vol. 2016-May, pp. 2714–2719, 2016, doi: 10.1109/APEC.2016.7468247.
[9] P. C. Dastagiri Goud, A. Sharma, and R. Gupta, "Solar PV Fed Fast Charging Converter with Isolated Unidirectional Dual-Bridge Topology," India Int. Conf. Power Electron. IICPE, vol. 2018-Decem, pp. 1–5, 2018, doi: 10.1109/IICPE.2018.8709492.
[10] N. Hassanzadeh, F. Yazdani, S. Haghbin, and T. Thiringer, "Design of a 50 kW phase-shifted full-bridge converter used for fast charging applications," 2017 IEEE Veh. Power Propuls. Conf. VPPC 2017 - Proc., vol. 2018-Janua, pp. 1–5, 2018, doi: 10.1109/VPPC.2017.8330881.
[11] L. Tan, B. Wu, and S. Rivera, "A bipolar-DC-bus EV fast charging station with intrinsic DC-bus voltages equalization and minimized voltage ripples," IECON 2015 - 41st Annu. Conf. IEEE Ind. Electron. Soc., pp. 2190–2195, 2015, doi: 10.1109/IECON.2015.7392426.
[12] V. M. Iyer, S. Gulur, G. Gohil, and S. Bhattacharya, "An approach towards extreme fast charging station power delivery for electric vehicles with partial power processing," IEEE Trans. Ind. Electron., vol. 67, no. 10, pp. 8076–8087, 2020, doi: 10.1109/TIE.2019.2945264.
[13] B. Hussein, N. Abdi, and A. Massoud, "Development of a three-phase interleaved converter based on SEPIC DC–DC converter operating in discontinuous conduction mode for ultra-fast electric vehicle charging stations," IET Power Electron., vol. 14, no. 11, pp. 1889–1903, 2021, doi: 10.1049/pel2.12157.
[14] A. C. Nair and B. G. Fernandes, "Solid-State Transformer Based Fast Charging Station for Various Categories of Electric Vehicles with Batteries of Vastly Different Ratings," IEEE Trans. Ind. Electron., vol. 68, no. 11, pp. 10400–10411, 2021, doi: 10.1109/TIE.2020.3038091.
[15] G. Town, S. Taghizadeh, and S. Deilami, "Review of Fast Charging for Electrified Transport: Demand, Technology, Systems, and Planning," Energies, vol. 15, no. 4, 2022, doi: 10.3390/en15041276.
[16] A. V. J. S. Praneeth and S. S. Williamson, "A Review of Front End AC-DC Topologies in Universal Battery Charger for Electric Transportation," 2018 IEEE Transp. Electrif. Conf. Expo, ITEC 2018, pp. 916–921, 2018, doi: 10.1109/ITEC.2018.8450186.
[17] M. Gierczyński et al., "Design of DC/DC converter in dual active bridge (DAB) topology for application in a lithium-ion battery test setup," Przeglad Elektrotechniczny, vol. 97, no. 3, pp. 77–81, 2021, doi: 10.15199/48.2021.02.19.
[18] Y. Yan, H. Gui, and H. Bai, "Complete ZVS Analysis in Dual Active Bridge," IEEE Trans. Power Electron., vol. 36, no. 2, pp. 1247–1252, 2021, doi: 10.1109/TPEL.2020.3011470.
[19] K. Najdek, "Use of the D-decomposition technique for gains selection of the Dual Active Bridge converter output voltage regulator," Przeglad Elektrotechniczny, no. 11, pp. 268–273, 2019, doi: 10.15199/48.2019.11.61.
[20] T. Gajowik, K. Rafał, and M. Bobrowska-Rafał, "Bi-directional DC-DC converter in three-phase Dual Active Bridge Topology," Przeglad Elektrotechniczny, vol. 90, no. 5, pp. 14–19, 2014, doi: 10.12915/pe.2014.05.03.
[21] V. M. Iyer, S. Gulur, G. Gohil, and S. Bhattacharya, "An approach towards extreme fast charging station power delivery for electric vehicles with partial power processing," IEEE Trans. Ind. Electron., vol. 67, no. 10, pp. 8076–8087, 2020, doi: 10.1109/TIE.2019.2945264.